Pergamon

Acta Materialia 50 (2002) 1951–1960

Acta MATERIALIA

www.actamat-journals.com

A study of alloying behaviour in the Ti–Al–V system

S. Diplas [a], P. Tsakiropoulos [a,*], G. Shao [a], J.F. Watts [a], J.A.D. Matthew [b]

[a] *School of Engineering, University of Surrey, Guildford, Surrey, GU2 7XH, UK*
[b] *Department of Physics, University of York, Heslington, York Y01 5DD, UK*

Received 18 June 2001; accepted 20 December 2001

Abstract

High-energy and conventional X-ray photoelectron spectroscopy (XPS) with Cr K_β ($h\nu$ = 5946.7 eV) and Al K_α ($h\nu$ = 1486.6 eV) radiation, respectively, were used to calculate the Auger parameters of Al, Ti and V in the Ti–Al (Al = 10, 20, 30 at%), Ti–35 at% Al–15 at% V, Ti–40 at% Al–20 at% V, Ti–25 at% Al–25 at% V and Ti–50 at% V alloys. The shifts of the Auger parameters of the elements between unalloyed and alloyed conditions were used to explain electronic changes occurring upon alloying and were related to the thermodynamics and the microstructures of the alloys. The large negative shift of the Al Auger parameter indicated that Al atoms are better screened in the pure metal environment than in the alloys. This shift was also related to ordering in the Ti–Al and Ti–Al–V alloys. The Auger parameter differences of the transition metals were small and either within or very close to the experimental error, which is in agreement with previous studies.

Keywords: Alloys; X-ray photoelectron spectroscopy (XPS); Auger parameter; Alloying behaviour

1. Introduction

Alloy design is gradually shifting away from empirical practices by using systematic and more cost-effective methods [1]. Two approaches for alloy development involve thermodynamic modelling based on CALPHAD [1,2] and "ab-initio" or first-principles calculations (FPC) [3]. Thermodynamic modelling is a phenomenological approach and is based on optimisation of experimental data. CALPHAD provides valuable information on phase equilibria but its use is limited by the difficulty in producing data on lattice stabilities of metastable phases. The latter can be overcome by using FPC, which can also be used to study alloying behaviour at the level of electrons. However, data produced by FPC lack sufficient accuracy for practical applications at temperatures above absolute zero.

Alloy phase formation at the atomic scale involves coexistence of atoms from two or more different elements in the same lattice accompanied with electronic changes in the valence configurations, which lead to the formation of new bonds or modification of the existing ones. Thus the crystal structure may be modified or completely altered, and these modifications may trigger microstruc-

* Corresponding author.
E-mail address: p.tsakiropoulos@surrey.ac.uk (P. Tsakiropoulos).

1359-6454/02/$22.00
PII: S1359-6454(02)00038-1

tural changes with significant impact on the properties and performance of the alloys formed. This interplay between atomic structure↔crystal structure↔microstructure↔material performance justifies the increasing necessity for a better understanding of alloying at the electronic level.

In previous studies [4–8], X-ray photoelectron spectroscopy (XPS) data such as Auger parameter values, and plasmon energies and intensities have been used to gain a better understanding of the alloying behaviour of elements in terms of the nature of atomic bonding, crystal structure modifications and microstructural evolution. In this paper an attempt has been made to understand the phenomena taking place at the atomic and subatomic level upon alloying via information obtained by electron spectroscopy and to relate these observations to the microstructures of alloys of the Ti–Al, Ti–V and Ti–Al–V alloy systems.

2. Experimental

Alloys of nominal composition Ti–10, 20 and 30 at% Al, Ti–35 at% Al–15 at% V, Ti–40 at% Al–20 at% V, Ti–25 at% Al–25 at% V and Ti–50 at% V were prepared by clean melting using high-purity Ti, V and Al. During melting special care was taken to ensure chemical homogeneity and very low levels of interstitials (O_2<500 wppm, H_2<20 wppm, C<20 wppm and N_2<30 wppm, analysis by TIMET). The surfaces of the alloys were polished down to 1 μm followed by ultrasonic cleaning with inhibisol. The polished samples were then analysed by XPS.

Acquisition of deep-well-localised 1s–KLL transitions lead to optimum results in Auger parameter studies. Although these transitions are inaccessible for many important elements using conventional sources, this problem can be circumvented by using a high-energy monochromated source, such as the combined Al K_α (1486.6 eV) and Cr K_β (5946.7 eV) source available on the Scienta ESCA 300 spectrometer at the CLRC Daresbury Laboratory [9,10]. The Cr K_β source was used in this study to probe the high-energy 1s and KLL features of Ti, V and Al [4,5,7–10].

After the ex situ preparation, the samples were cleaned within the spectrometer by Ar^+ bombardment (40 μA for 15 min) prior to analysis. The spectra were acquired at a pass energy of 300 eV with the sample surface normal to the analyser electron optics. Both the data acquisition and subsequent analysis were performed using the PC-based SCIENTA software. Peaks were fitted using Voigt functions on a Shirley background, with both the peaks and the background being optimised during the peak-fitting process.

The final state and the initial state Auger parameter values were acquired in order to separate the influence of initial and final state effects on the Auger parameter changes. The final state Auger parameter (α^*) [11] was calculated by adding the binding energy (*BE*) level of the photoelectron peak to the kinetic energy (*KE*) level of the equivalent Auger transition according to Eq. (1):

$$\alpha^* = BE_{\text{photoelectron}} + KE_{\text{Auger electron}} \quad (1)$$

The Auger parameter measured from eq. (1) can be determined accurately since energy referencing problems are cancelled out.

The initial state Auger parameter (β) [12] is given by Eq. (2):

$$\beta = KE_{(ijj)} + BE_{(i)} + 2BE_{(j)} \quad (2)$$

where $KE_{(ijj)}$ is the kinetic energy of the Auger transition involving the *i* and *j* core levels, and $BE_{(i)}$ and $BE_{(j)}$ are the binding energies of the *i* and *j* core levels, respectively. The initial state Auger parameter does not have the advantages arising from the cancellation of energy referencing errors. However, this limitation may be minimised when simultaneous observations of spectra from two different environments are made.

It can be shown that the differences between the Auger parameters of an element in two different environments are [12–15]

$$\Delta\alpha^* = 2\Delta R \quad (3)$$

and

$$\Delta\beta = 2\Delta V, \quad (4)$$

where *R* is the final state relaxation energy and *V* is the atomic core potential. Thus, Eqs. (3) and (4) demonstrate how initial and final state effects can be separated.

These relationships are only strictly valid when the environmental shift is the same for all levels concerned. A full data set is not available for all elements under consideration currently, although it has been shown, using monochromated Ag L_α radiation, that such an equivalence does exist for the Al 1s and Al 2p levels in metallic Al and Al_2O_3 [16].

3. Results

The microstructures of the alloys [17–19] are summarised in Table 1. The diffuse ω structure was present in the body-centred cubic (bcc) type parent phases (A2 or B2 structures) [20]. Chemical ordering occurs in the solid-solution phases such as the hexagonal close-packed (hcp) (A3→DO_{19}) and the bcc (A2→B2) structures, mainly due to the negative interaction between Ti and Al [19]. Ordering energy values for the A2→B2 transition are given in Table 2 [19].

Figs. 1–7 show representative survey spectra and photoelectron and Auger peaks used for the Auger parameter calculations. The reduction in intensity and the broadening of the Al 1s plasmon peaks (Fig. 5) in the alloys compared with the pure metals should be noticed. Table 1 shows the difference in both the initial and final state Auger parameter values between pure metal and alloy for Ti, V and Al. It also shows the difference in the values of the final state Auger parameters acquired from the Al K_α excited Al 2p and Al KLL as well as the differences in binding energy of the Al 2p levels between pure metal and alloy. The Auger parameter differences (alloy relative to the pure metal) of the transition metals (Ti, V) were smaller than the Auger parameter differences of Al (see Table 1). This is in agreement with previous observations [4–8]. As can been seen from Table 1, the differences in the initial state Auger parameters were always larger than the differences in the final state Auger parameters, indicating the occurrence of initial state effects such as charge transfer from the Al sites towards the Ti and/or V sites. This is supported further by the observation that the shifts of the Al 1s binding energy were always larger than

Table 1
Differences in initial and final state Auger parameters as well as differences in the binding energy levels of the photoelectron peaks of Al, Ti and V between alloyed and unalloyed states. The negative sign implies a decrease of the Auger parameter or binding energy in the alloy compared with the metal

	Ti–10Al	Ti–20Al	Ti–30Al	Ti–50V	Ti–25V–25Al	Ti–15V–35Al	Ti–20V–40Al
Al							
$\Delta\alpha$[a]	−0.9	−0.7	−0.7		−0.7	−0.6	−0.6
ΔE_B, Al 1s[b]	−1.1	−1.0	−0.9		−1.0	−0.9	−0.8
$\Delta\beta$[c]	−2.1	−1.8	−2.1		−2.5	−2.1	−2.0
ΔE_B, Al 2p[d]	−0.6	−0.6	−0.7				
Ti							
$\Delta\alpha$[a]	−0.1	0.0	+0.1	−0.3	−0.2	−0.1	−0.1
ΔE_B, Ti 1s[b]	−0.3	−0.1	−0.1	−0.3	−0.2	−0.1	−0.1
$\Delta\beta$[c]	−0.4	−0.2	−0.5	−0.5	−0.3	−0.2	−0.1
V							
$\Delta\alpha$[a]				+0.3	0.0	−0.1	−0.1
ΔE_B, V 1s[b]				+0.2	−0.1	0.0	−0.1
$\Delta\beta$[c]				+0.3	−0.2	−0.5	−0.5
Structure	A3 (hcp)	α_2—DO_{19} (ordered)+A3	α_2—DO_{19}	A2 (bcc)	B2 (ordered) (bcc)		

[a] Difference in final state Auger parameter between pure metal and alloy (error = ± 0.15 eV).
[b] Difference in binding energy of Al 1s, V 1s or Ti 1s between pure metal and alloy (error = ± 0.1 eV).
[c] Difference in initial state Auger parameter between pure metal and alloy (error = ± 0.4 eV).
[d] Difference in binding energy of Al 2p between metal and alloy (error = ± 0.1 eV).

Table 2
Values of valence electron density, Al 1s plasmon energy, plasmon intensity ratios for pure aluminium and alloys, calculated plasmon energies and calculated A2→B2 ordering energies

Alloy	Valence electron density (10^{28} m^{-3})	Plasmon energy (experimental) (eV)	Plasmon energy (calculated) (eV)	Al 1s/1st plasmon intensity ratios (experimental values)	A2/B2 ordering energy (J/mol)
Pure Al	18.07[a]	15.3±0.14	15.8[a]	2:1	–
Ti–20at%Al	22.6	17.5±0.14	17.7	3.5:1	1400
Ti–30 at% Al	22.2	17.3±0.14	17.5	4.2:1	3150
Ti–25 at% V–25 at% Al	25.05	17.5±0.14	18.6	3.4:1	2852
Ti–15 at% V–35 at% Al	23.62	17.8±0.14	18.1	3.4:1	5167
Ti–20 at% V–40 at% Al	24.06	17.7±0.14	18.2	4:1	5595

[a] Values taken from [20].

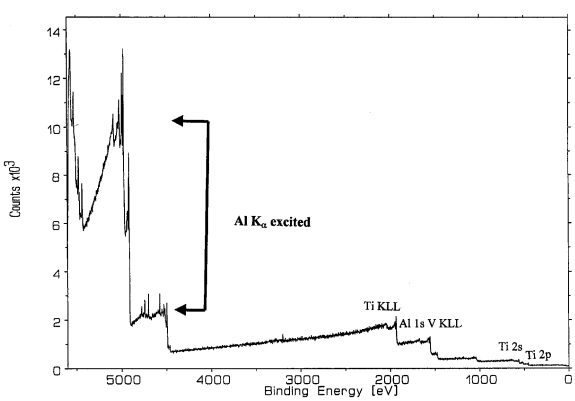

Fig. 1. XPS survey spectrum of the Ti–20 at% V–40 at% Al alloy excited by Cr K_β radiation. The Al K_α leakage radiation gives rise to a series of high. These regions of the spectrum are shown in more detail in Figs. 2 and 3.

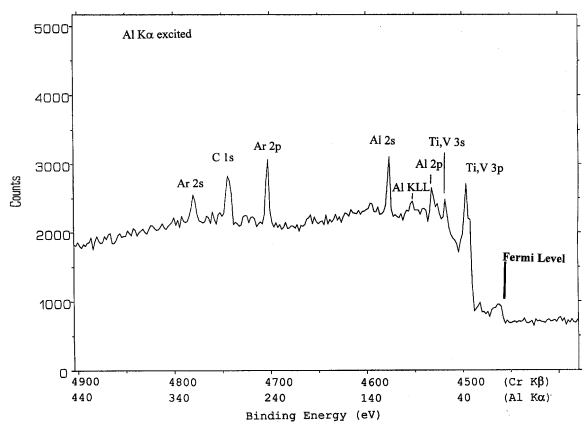

Fig. 2. Intermediate kinetic energy region of Fig. 1 identified with both a Cr K_β and an Al K_α binding energy scale. All XPS features in this region of the spectrum are associated with Al K_α excitation.

the final state Auger parameter differences. Although not shown in Table 1 for all alloys, the shifts of the Al 2p binding energy levels between pure metal and alloy were also significant, in contrast to the V and Ti 2p binding energy levels, for which the binding energy shifts were small.

As shown in Table 2, the intensities of the Al 1s, 2s and 2p plasmons in the Ti–Al and Ti–Al–V alloys decreased compared with the pure metal. In addition, a broadening of the plasmon peaks was observed in the alloys and the plasmon losses occurred at higher energies compared with the pure metal (Table 2). The plasmon energy calculations for the alloys were done as follows. First, multiplying the number of atoms of the different elements per unit cell by the total number of valence electrons per atom and dividing the product by the volume of the unit cell calculated the alloy valence electron density. The alloy plasmon energy was the product of the square root of the ratio of the alloy valence electron density to the pure metal valence electron density multiplied by the pure metal plasmon energy. The values for the pure Al valence electron density as well as the pure Al plasmon energy were taken from the literature [21]. Error limits in the above calculations could not be calculated due to lack of error values in the literature. For the calculation of the volumes of the unit cells

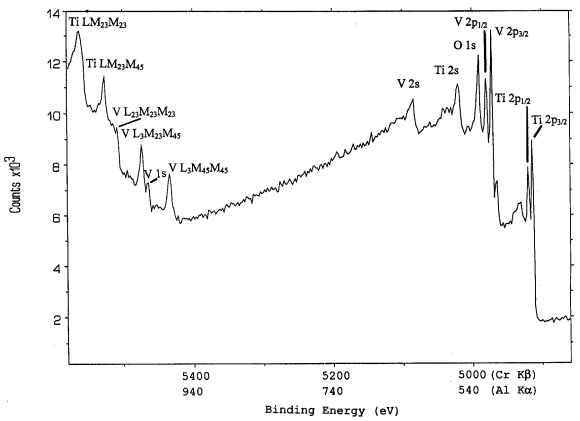

Fig. 3. Low-kinetic-energy region of Fig. 1 identified with both a Cr K_β and an Al K_α binding energy scale. The Cr K_β excited V 1s and Ti 1s core levels can be seen clearly at a binding energies of 5465 eV and 4965 eV, respectively

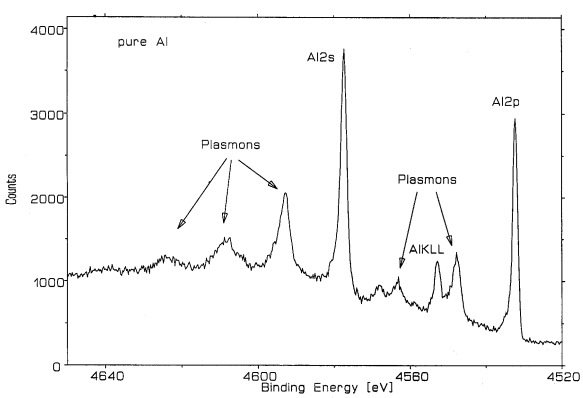

Fig. 4. Al K_α excited Al peaks used in the Auger parameter calculations.

of the alloys, the lattice parameter values were taken from [18] and [22].

4. Discussion

4.1. Auger parameter variations in the Ti–Al–V system

Auger parameter changes have been suggested to be a measure of the screening efficiency of a system in response to the presence of a localised core hole [23,24]. Considering that metals are

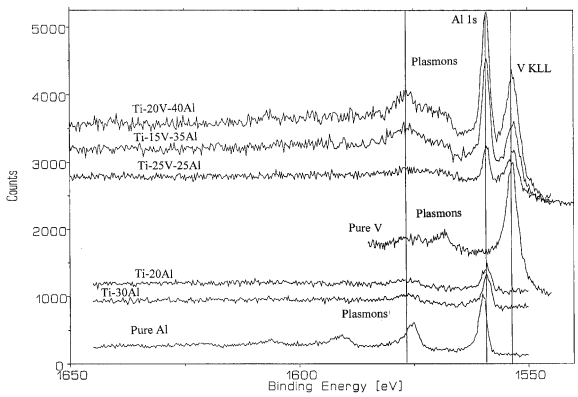

Fig. 5. Comparison of the Al 1s, V KLL peaks and their associated plasmon peaks of the alloys studied.

characterised by perfect screening, reduced screening means that the atoms experience a "less metallic" environment. The general observation of the Auger parameter variations (both initial and final state AP, Table 1) of the elements of interest, between pure metal and alloy, indicate that the metal with sp valence configuration (Al) is better screened in the elemental solid than in both the binary and ternary alloys.

The Auger parameters and the Al 1s binding energy, particularly of the ordered alloys, did not vary significantly with Al content. Both the small decrease of the AP variation and the variation in Al 1s binding energy with increasing Al content are attributed to the increased number of the Al atoms surrounding a single Al atom and the subsequent experience of a more familiar environment closer to the parent lattice of pure Al. However, one should be cautious, since this variation is close to or within the experimental error involved in measuring peak positions (±0.1 eV) and in determining the initial and final state Auger parameters (±0.4 and ±0.14 eV, respectively). The relatively large variation of the Al Auger parameter between pure metal and alloy is in agreement with previous studies of Auger parameters of ordered phases [4,5,7,12,25–27].

The variations of both initial and final state AP of the transition metals were small and either within or just outside the experimental errors, in agreement with previous studies [4–8]. Bearing in mind the reservation about the AP values being

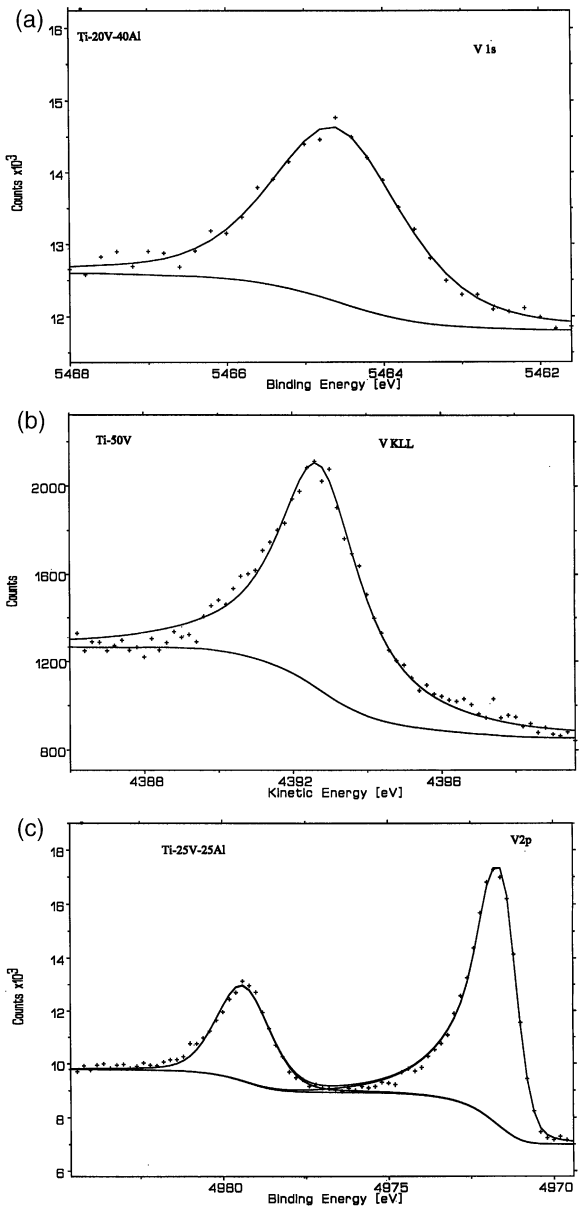

Fig. 6. High-resolution photoelectron and Auger peaks used in the Auger parameter calculations: (a) Cr K_β excited V 1s of the Ti–20 at% V–40 at% Al alloy, (b) Cr K_β excited V KLL of the Ti–50 at% V alloy and (c) Al K_α excited V 2p of the Ti–25 at% V–25 at% Al alloy.

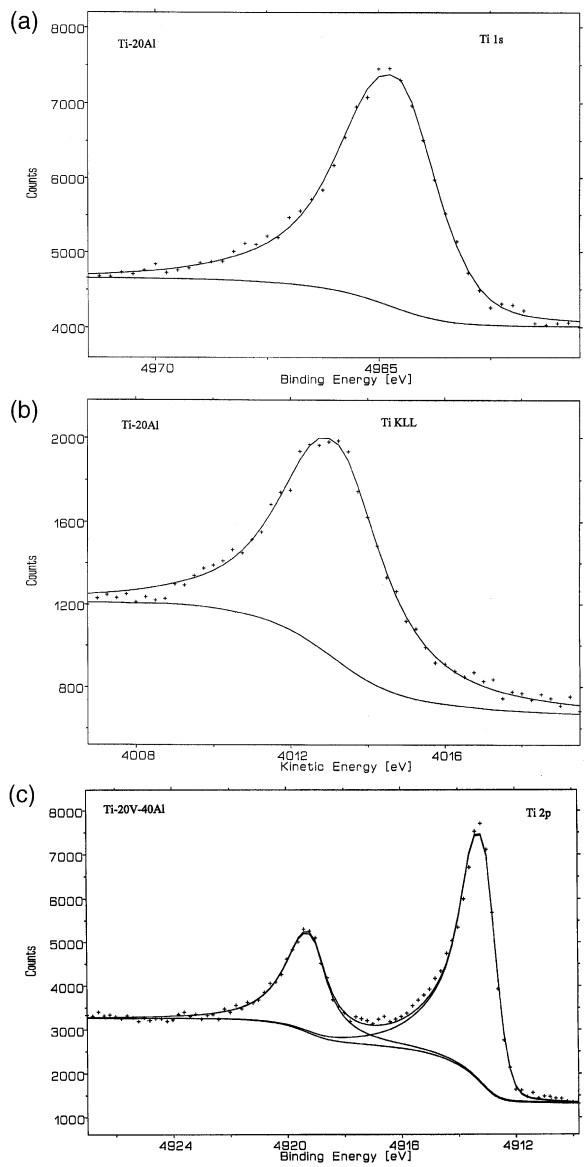

Fig. 7. High-resolution photoelectron and Auger peaks used in the Auger parameter calculations: (a) Cr K_β excited Ti 1s of the Ti–20 at% Al alloy, (b) Cr K_β excited V KLL of the Ti–20 at% Al alloy and (c) Al K_α excited Ti 2p of the Ti–20 at% V–40 at% Al alloy.

close to error limits, it seems that for Ti, as for Al, the screening efficiency in the presence of a core hole is reduced in the binary Ti–V alloy and possibly the ternary Ti–Al–V alloys. Despite the reservations because of the small AP variations for V, it may be suggested that V atoms are screened better, i.e. they experience a more "metallic" environment in the binary Ti–V alloy than in the pure metal but possibly not in the ternary Ti–Al–V alloys. Initial state effects such as charge transfer (or charge redistribution) may also be important, since in all cases the binding energy shifts in Al as well as the variation of the Al initial state Auger parameter were bigger than the changes in the Al final state Auger parameter.

4.2. Auger parameter and alloying behaviour in the Ti–Al–V system

Fig. 8 shows the values of final state AP differences of Al (in the binary Ti–Al and Al–V alloys and in the ternary Ti–Al–V alloys) as well as the values of final state AP differences of Ti and V in the binary Al–V and Ti–V alloys, on a calculated isothermal section (873 K) of the Ti–Al–V ternary

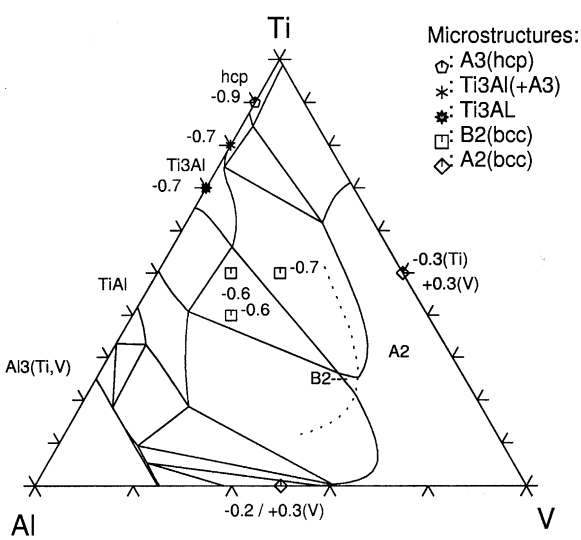

Fig. 8. Isothermal section (873 K) of the Ti–Al–V ternary system, showing values of Al AP differences (in the binary Ti–Al and V–Al and the ternary Ti–Al–V alloys) as well as values of Ti and V AP differences in the binary V–Al and Ti–V alloys. The dotted line delineates the A2/B2 phase boundary.

alloy system [18,19]. Thermodynamic modelling and microstructural studies have defined the regions of ordered and disordered phases [17–20]. The A2 → B2 ordering energies at 300 K are given in Table 2 for the different alloy compositions. The Ti–Al alloy system is characterised by a strong ordering tendency and the formation of ordered Ti–Al phases when the Al content exceeds 10 at% [19] (see also Table 1 and Fig. 8). The Ti–Al–V alloys of this study are in the phase field of the B2 ordered phase, whilst the Ti–50 at% V and the Al–50 at% V alloys had a disordered A2 crystal structure [4,5].

Atomic size differences and electrochemical factors can be used to explain the formation of ordered solid solutions. Ordering due to an unfavourable size factor may be interpreted as the result of the strain induced in the lattice by the different size between solute and solvent atoms, and the subsequent strain relaxation achieved by rearranging the positions of the solute atoms at fixed lattice sites so that the total energy of the crystal can be minimised. The lattice parameter of bcc V is 0.302 nm [28]. Since the stable structures of Al and Ti are face-centred cubic (fcc) and hcp rather than bcc, the effective lattice parameters of bcc Al and Ti must be calculated in order to consider the size factor. The lattice parameters of bcc Al and Ti have been calculated as 0.321 and 0.327 nm, respectively, by considering the effects of both packing fractions and coordination numbers of different structures [22]. The difference in atomic sizes between Al and V (+5.92%) is bigger than between Al and Ti (−1.87%). Furthermore, the difference in atomic sizes between Ti and V is bigger than between Al and Ti and between Al and V. Therefore, formation of ordered phases would be preferred in V–Al and Ti–V alloys, if the atomic size were the determining factor. However, this is not the case and, therefore, ordering must be favoured for another reason.

According to the electrochemical factor, dissimilar atoms may be attracted if there is a substantial difference in electronegativity between them. In this case unlike neighbour bonds would be preferred. These bonds would be characterised by an increased ionicity compared with the bonds between like neighbours in a random solid sol-

ution, which would have a metallic character. The difference in electronegativity between Al and V is exactly the same as between Ti and V (0.1 units in the Pauling scale). Aluminium and Ti have the same electronegativity [29]. Therefore, the differences in electronegativity values cannot explain ordering in Ti–Al and Ti–Al–V alloys.

Auger parameter differences have been shown to be related to order or disorder phenomena in metallic alloys [4–7]. Ordered alloys that contain an element of s–p valence configuration (e.g. Al) exhibit large Auger parameter differences of the s–p metal between alloyed and unalloyed states compared with its Auger parameter variations in disordered alloys. Large AP differences were observed in the Ti–Al and Ti–Al–V alloy systems, which are characterised by a strong ordering tendency. The large AP shift of Al in the Ti–10 at% Al alloy, which has a disordered A3 crystal structure but lies close to the boundary between order/disorder transition, may be indicative of the ordering tendency. Moreover, the large shift in the Auger parameters (both initial and final state) in the Ti–10 at% Al alloy may be attributed to the fact that the Al atoms exist in an environment of increased number of Ti atoms in the alloy. However, there is some uncertainty about the exact position of the Al 1s, Al 2p and Al KLL peaks owing to the low Al content of the alloy, and this should not be underestimated.

The initial state charge transfer in the alloys is possibly significant (as suggested by the difference between the initial and final state AP differences in Table 1) but such effects may also be attributed to the formation of directional bonding between Al and Ti, which could probably cause a significant charge redistribution. The formation of such directional bonding could be responsible for the chemical order in the Ti–Al alloys. Ordering in the Ti–Al solid solutions is characterised by a significant decrease of the lattice parameter of Al (negative deviation from the Vegard's law) in Ti–Al alloys [22]. The decrease of the Al lattice parameter may be explained in terms of valence electron transfer from the Al sites to the neighbouring Ti sites via the formation of directionally covalent Ti–Al bonding orbitals. Research on ordered transition metal aluminides has indicated the existence of a strong covalent bonding component, which makes the bonding between transition metal (TM) and Al atoms significantly stronger than between TM–TM or Al–Al atoms [30]. The increased bond strength results in a shortening of the length of the TM–Al bond, which in turn implies a decrease of lattice parameter upon ordering [31].

Similar conclusions can also be reached when initial state effects are explained in the framework of the "jellium approximation" [32]. As is shown in Table 2, the valence electron density of pure Al is significantly lower than the valence electron density in the binary and ternary alloys, which is increased due to the presence of the transition metals Ti and V. Aluminium atoms in the parent lattice experience a lower valence electron density than in the lattice of the alloys. Minimisation of their embedding energy in the Ti lattice of the alloys (where the valence electron density around the Al sites is high) would require electron transfer away from the Al atoms. This electron "donation" from Al to Ti (and/or V) during the introduction of Al into Ti leads to a decreased lattice parameter of Al and results in the observed negative deviation of the Al size from Vegard's law [22], as discussed above.

The above interpretations of the observed AP changes on alloying can explain the variations of lattice parameters in the Ti–Al alloys. However, the situation is more complicated in the ternary alloys due to further difficulties arising from the coexistence of atoms of the two transition elements (Ti and V) and the subsequent hybridisation occurring in the bonding between these elements and the Al atoms.

4.3. Plasmon energy and lattice parameters in Ti–Al and Ti–Al–V alloys

Fig. 5 and Table 2 show an increase in energy and a decrease in intensity of the Al 1s plasmon satellites. It is known that the higher the plasmon intensity, the more "free" the valence electrons are in the solid [33]. In our case, the s–p type valence electrons of Al seem to be more strongly bound in the alloys than in the pure metal, possibly through hybridised bonds with the Ti (in Ti–Al) and/or the Ti and V (in Ti–Al–V alloys) valence electrons.

This is probably the reason why the plasmon peaks are less intense in the alloys. This strong bonding between Ti–Al and Ti–Al–V atoms is reflected in the decrease of the Ti lattice parameters with increasing Al additions [22] or with increasing V and Al additions [18,20]. This decrease is significant in the Ti–20 at% V–40 at% Al alloy, which has the smallest lattice parameter (0.316nm) (the lattice parameters of Ti–25 at% V–25 at% Al and Ti–15 at% V–35 at% Al are 0.317 and 0.318 nm, respectively [18]), and is characterised by the biggest decrease in plasmon intensity (see Table 2), which is indicative of the strong bonding of the sp valence electrons.

In both the binary and ternary alloys the plasmon satellites of the Al 1s occur within the same energy range (17.5–18 eV). The plasmon energy is, in the simplest approximation, proportional to the square root of the density of "quasi free" electrons and this is consistent with the increase in the sp valence electron density in the unit cells of Ti–Al and Ti–Al–V alloys (see Table 2). Moreover, as chemical order in the Ti–Al–V alloys is largely attributed to the formation of strong covalent bonds [34], it is not surprising that the Al plasmon peak intensity in the Ti–Al–V alloys, where chemical order occurred, decreased with respect to the pure element. The calculated plasmon energies for Ti–Al and Ti–Al–V alloys (see Table 2) are in good agreement with the experimental values.

Combining the data from the Auger parameter studies and the plasmon intensity pattern the following picture emerges: although there is an enhanced average valence electron density resulting in higher plasmon energies, the electrons in the sp–TM d bands are much more localised in character and participate less strongly in the many electron plasmon excitations. The fact that these bands are less polarisable than "quasi free" electrons may be the reason for the reduced Al core electron screening efficiency, as opposed to explanations involving charge transfer. The combination of these two types of electron spectroscopic data therefore gives valuable insights into the electronic environment of these alloys.

5. Conclusions

The 1s, 2p photoelectron core levels and the KLL and LMM Auger transitions were used to calculate the Auger parameters of Al, Ti and V in binary Ti–Al, V–Al and Ti–V and ternary Ti–Al–V alloys. Alloying behaviour in the Ti–Al–V system has been discussed using the Auger parameter values and plasmon losses. Large AP variations of the sp metal (Al) were attributed to chemical order in the alloys. Changes in the lattice parameters of the alloys were related to the initial state charge transfer and the plasmon intensities.

Acknowledgements

We are grateful to Dr G. Beamson for assistance with the experiments using Cr K_β excitation. We also acknowledge the support by EPSRC (GR/M15101) for the use of the high-energy XPS facility at RUSTI, Daresbury. Fruitful discussions with Professor J.E. Castle and Professor P. Weightman are also gratefully acknowledged.

References

[1] Nash P, Sundman B. In: Nash P, Sundman B, editors. Applications of thermodynamics in the synthesis and processing of materials. Warrendale (PA): TMS; 1995.
[2] Saunders N, Miodownik AP. CALPHAD: a comprehensive guide, Pergamon Materials Series. Oxford: Pergamon, 1998.
[3] Pettifor DG, Cottrell AH, editors. Electron theory of metals and alloys. London: The Institute of Materials; 1992.
[4] Diplas S, Shao G, Morton SA, Tsakiropoulos P, Watts JF. Intermetallics 1999;7:937.
[5] Diplas S, Shao G, Tsakiropoulos P, Watts JF, Matthew JAD. Surf. Interf. Anal. 2000;27:65.
[6] Diplas S, Tsakiropoulos P, Brydson RMD, Watts JF. Phil. Mag. A 1998;77:1067.
[7] Arvanitis A, Diplas S, Tsakiropoulos P, Watts JF, Morton SA, Whitting M et al. Acta Mater. 2001;49:1063.
[8] Mitchell T, Diplas S, Tsakiropoulos P, Watts JF, Matthew JAD. Phil Mag A 2002;82(4):841–55.
[9] Morton SA, Beamson G, Watts JF, Clark DT, Castle JE. In: Mathieu HJ, Reihl B, Briggs D, editors. Proceedings of ECASIA 95, 6th European Conference on Applications of Surface and Interface Analysis. Chichester: John Wiley and Sons; 1996. p. 102-3.

[10] Diplas S, Watts JF, Morton SA, Beamson G, Tsakiropoulos P, Clark DT, et al. J Electron Spectrosc Relat Phenom 2001;113:153–66.
[11] Gaarenstroom SW, Winograd NJ. J. Chem. Phys 1997;67:500.
[12] Evans JA, Laine AD, Weightman P, Matthew JAD, Woolf DA, Westwood DI et al. Phys. Rev. B 1992;46:1513.
[13] Weightman P. J. Electron Spectrosc. Relat. Phenom. 1998;93:165.
[14] Thomas TD. J. Electron Spectrosc. Relat. Phenom. 1980;20:117.
[15] Cole RJ, Brooks NJ, Weightman P, Matthew JAD. Phys. Rev. B 1995;52:2976.
[16] Edgell MJ. Ph.D. thesis, University of Surrey, Guildford, 1986.
[17] Ahmed T, Flower HM. Mater. Sci. Technol. 1994;10:272.
[18] Shao G, Tsakiropoulos P, Miodownik AP. Intermetallics 1995;3:315.
[19] Shao G, Tsakiropoulos P. Mater. Sci. Eng. 1996;A216:1.
[20] Shao G, Miodownik AP, Tsakiropoulos P. Phil. Mag. A 1995;71:1389.
[21] Myers HP. Introductory solid state physics, 2nd ed. London: Taylor & Francis, 1990.
[22] Shao G, Tsakiropoulos P. Mater. Sci. Eng. 1999;A271:286.
[23] Matthew JAD, Morton SA, Walker CGH, Beamson G. J. Phys. D: Appl. Phys. 1995;28:1702.
[24] Walker CGH, Morton SA, Beamson G, Matthew JAD, Yousif FN. J. Electron Sprectrosc. Relat. Phenom. 1994;70:73.
[25] Thomas TD, Weightman P. Phys. Rev. B 1986;33:5406.
[26] Weightman P, Cole RJ, Brooks NJ, Thornton JMC. Nucl. Instrum. Meth. Phys. Res. B 1995;97:472.
[27] Kövér L, Kovács Zs, Sanjinés R, Weightman P, Margaritondo G, Varga D et al. In: Matthew HJ, Rheihl B, Briggs D, editors. Proceedings of ECASIA 95, 6th European Conference on Applications of Surface and Interface Analysis. Chichester: John Wiley & Sons; 1996. p. 448–51.
[28] Pearson WB. Handbook of lattice spacings and structures of metals, vol. 2. Ontario, Canada: Pergamon Press, 1967.
[29] Ellis H, editor. Book of data, Nuffield Advanced Science. London: Longman; 1986.
[30] Nguyen-Manh D, Pettifor DG. Intermetallics 1999;7:1095.
[31] Cahn RW. Intermetallics 1999;7:1089.
[32] Cottrell A. Concepts in the electron theory of alloys. London: IOM Communications Ltd, 1998.
[33] Egerton RF. Electron energy-loss spectroscopy in the electron microscope, 2nd ed. New York: Plenum Press, 1996.
[34] Nguyen-Manh D. University of Oxford, private communication to the authors.